

On the Cooling Trend of SGR 0526–66

Tolga Güver¹, Ersin Göğüş¹ and Feryal Özel²

¹*Sabancı University, Faculty of Engineering and Natural Sciences, Orhanlı Tuzla 34956 Istanbul Turkey*

²*Department of Astronomy, University of Arizona, 933 N. Cherry Ave., Tucson, AZ 85721*

ABSTRACT

We present a systematic analysis of all archival Chandra observations of the soft-gamma repeater SGR 0526–66. Our results show that the X-ray flux of SGR 0526–66 decayed by about 20% between 2000 and 2009. We employ physically motivated X-ray spectral models and determine the effective temperature and the strength of the magnetic field at the surface as $kT = 0.354_{-0.024}^{+0.031}$ keV and $B = (3.73_{-0.08}^{+0.16}) \times 10^{14}$ G, respectively. We find that the effective temperature remains constant within the statistical uncertainties and attribute the decrease in the source flux to a decrease in the emitting radius. We also perform timing analysis to measure the evolution of the spin period and the period derivative over the nine year interval. We find a period derivative of $\dot{P} = (4.0 \pm 0.5) \times 10^{-11}$ s s⁻¹, which allows us to infer the dipole magnetic field strength and compare it with the one determined spectroscopically. Finally, we compare the effective temperature of SGR 0526–66 with the expected cooling trends from magnetized neutron stars and suggest an initial magnetic field strength of 10^{15-16} G for the source.

Key words: stars: neutron - X-ray: individual

1 INTRODUCTION

Soft Gamma Repeaters (SGRs) and Anomalous X-ray Pulsars (AXPs) are the prime representatives of magnetars – a class of neutron stars that are thought to be powered by the decay of their superstrong magnetic fields ($B \sim 10^{14} - 10^{15}$ G, Duncan & Thompson 1992). Aside from emitting energetic bursts in hard X-rays and soft gamma rays, magnetars are bright X-ray sources ($L_x \sim 10^{33} - 10^{36}$ erg s⁻¹), emitting pulsed X-rays either persistently or episodically (see Woods & Thompson 2006 and Mereghetti 2008 for detailed reviews). X-ray observations of most of SGRs and AXPs over the last thirty years have shown that these sources are not steady emitters, exhibiting flux variability generally in conjunction with bursting activities (see e.g., Rea & Esposito 2011).

All known SGRs have been discovered when they went into a bursting phase, during which they emit repeated energetic bursts in soft gamma-rays. SGR 0526–66 was not an exception: it was discovered as the first SGR with an extremely bright gamma-ray burst on 1979 March 5 that was followed by a tail emission clearly pulsating at 8.1 s (Mazets et al. 1979). The burst location is within the supernova remnant, N49 in the Large Magellanic Cloud (Evans et al. 1980). The source exhibited 16 more bursts until 1983 April 5 with much lower intensity than that of the March 5th event (Aptekar et al. 2002). Since then, no bursts have been detected from SGR 0526–66.

Due to its large distance and the fact that the source is embedded in a supernova remnant, spectral and timing studies of SGR 0526–66 have been limited. The persistent X-ray source was identified with ROSAT, yielding the earliest view of the source as it is in burst quiescence (Rothschild, Kulkarni & Lingenfelter 1994). SGR 0526–66 has been the target of two Chandra X-ray Observatory (CXO) observations in 2000 and 2001. Thanks to the superb angular resolution of CXO, X-ray spectroscopy and timing investigations of the persistent source became possible. Based on these observations, spin period of ≈ 8.04 s was measured and a tentative \dot{P} of $\approx 6.5 \times 10^{-11}$ s s⁻¹ was inferred (Kulkarni et al. 2003). X-ray spectrum of the SGR 0526–66 could be described well with the empirical model of an absorbed blackbody plus a power law component. The resulting power law index was much steeper than that of other SGRs, while it was similar to the power law indices of AXPs, which led Kulkarni et al. (2003) to suggest that SGR 0526–66 is in a transition from the SGR-like phase to an AXP-like phase.

SGR 0526–66 and its associated supernova remnant, N49 was recently observed with XMM-Newton. Tiengo et al. (2009) reported that the X-ray spectrum of the source does not show any significant changes compared to XMM-Newton observations performed in 2000 and 2001 and SGR 0526–66 is still a bright persistent source, emitting at an X-ray luminosity of $\approx 4 \times 10^{35}$ erg s⁻¹. Very recently, Park et al. (2012) provided an in depth analysis of the supernova rem-

Table 1. Chandra Observations of the SGR 0526–66.

Date	Observation ID	Exposure (ks)
2000-01-04	747	43.9
2001-08-31	1957	53.4
2009-07-18	10123	28.2
2009-07-31	10808	30.2
2009-09-16	10807	27.3
2009-09-19	10806	27.9

nant using four Chandra observations that were obtained in 2009. They refined the Sedov age of N49 as $\tau_{\text{Sed}} \approx 4800$ yr. Park et al. (2012) also analysed the X-ray spectra of SGR 0526–66 using phenomenological models, such as the sum of a blackbody and a power-law or two blackbody models. They find that the X-ray flux of SGR 0526–66 varied by about 15 % between the observations performed in 2000/2001 and 2009. Further including archival ROSAT observations they detect a decay in X-ray flux by about ≈ 20 –30% for the last 17 years.

Here, we report on our systematic analysis of all archival Chandra observations of SGR 0526–66 to unveil the X-ray spectral characteristics of the source when it is in deep burst quiescence. We model the X-ray spectra with the Surface Thermal Emission and Magnetospheric Scattering (STEMS) model (Güver et al. 2007, 2008, 2011), to determine the effective surface temperature, the surface magnetic field strength, and the long term X-ray flux of SGR 0526–66. We also perform timing analysis to construct the spin period evolution of the source and obtain the inferred dipole magnetic field strength. Finally, we compare our results with the expected cooling trends from magnetized neutron stars.

2 OBSERVATIONS AND DATA ANALYSIS

We list the observations used in our study in Table 1. Note that there are two more Chandra observations that contain SGR 0526–66 in the field of view. However, the source was observed off-axis by about $4''$ in one of the observations (ObsID: 1041). The effects of vignetting do not allow a reliable source extraction without any contribution from the supernova remnant. The other observation (ObsID: 2515) has only 7 ks of effective exposure, that is too short to provide high enough signal-to-noise X-ray spectrum. Therefore, we exclude these two pointings from our investigations.

We reprocessed all of the observations with the CIAO software suit, version 4.2 and CALDB 4.3.0 using the recently introduced *chandra_repro*¹ tool. This tool automates the creation of new bad pixel file and level 2 event file. We applied barycentric correction to each event file using the *axbary* tool. To extract source spectra and lightcurves we selected a circular region centering the neutron star with a radius of $2''$, as shown in Figure 1. For the background we used an annular region that is centered on the coordinates of the neutron star and covers the range starting from $2.5''$ to $5''$ from the center. Finally, we selected data from a larger

annular region: centered on the neutron star and covering the range starting from $4''$ to $11''$, to generate an X-ray spectrum of the SNR and obtain an independent measurement of the hydrogen column density, as detailed below. Source and SNR extraction regions are shown in Figure 1. We extracted X-ray spectra using the *specextract* tool and created response files with the *mkacisrmf* and *mkarf* tools. We grouped each spectrum to have at least 50 counts per spectral channel.

3 X-RAY SPECTRAL ANALYSIS

We fit the data with XSPEC version 12.5.1n, using the Surface Thermal Emission and Magnetospheric Scattering and assumed a reference gravitational redshift of 0.306 for the neutron star. We calculated the unabsorbed fluxes in the 0.5 to 6.5 keV energy range using the *cfux* model in XSPEC. The distance of the SGR is assumed to be 48.1 kpc (Macri et al. 2006). Uncertainties reported throughout the paper correspond to 68% confidence limits of parameters, unless indicated otherwise.

Uncertainties in the amount of interstellar absorption of X-ray photons often hampers efforts to precisely determine the intrinsic spectral shape of these sources. Furthermore, as a free parameter, hydrogen column density becomes strongly correlated with the determined temperature of the X-ray source essentially affecting the resulting best fit value (see, e.g. Durant & van Kerkwijk 2006 and Güver et al. 2012 for a detailed discussion). Therefore, an accurate estimation of the hydrogen column density is crucial to deduce the spectral characteristics of the source. The fact that SGR 0526–66 is embedded in the supernova remnant N49 presents an advantage in this respect because it is possible to obtain an independent measurement of the hydrogen column density using the SNR. For that purpose, we extracted a SNR spectrum from the longest exposure and modeled it. Similar to the earlier studies of N49 (Park et al. 2003; Bilikova 2007; Tiengo et al. 2009; Park et al. 2012), we fit the remnant with a two component model, consisting of two plane-parallel shocked plasma functions (Borkowski et al. 2001, *vpshock* in XSPEC) both absorbed by the interstellar medium, assuming a solar abundance as given by Anders & Grevesse (1989). We obtained an adequate fit with a $\chi^2_{\nu} = 1.44$ for 99 degrees of freedom. We note that the relatively high χ^2 is mostly due a small number of individual energy bins, which could be emission lines that can not be resolved by the ACIS-S detector. Our best fit parameters are: $N_{\text{H}} = (0.15 \pm 0.03) \times 10^{22} \text{ cm}^{-2}$, $kT_1 = 0.54 \pm 0.01 \text{ keV}$, $\tau_1 > 3.6 \times 10^{13} \text{ s cm}^{-3}$, $kT_2 = 1.11 \pm 0.4 \text{ keV}$, $\tau_2 = (1.21 \pm 1.1) \times 10^{10} \text{ s cm}^{-3}$, where kT_1 , kT_2 , τ_1 and τ_2 denotes the temperature of the plasma and the upper limit on the ionization timescale for each component. The elemental abundances we found are as follows: $\text{Ne}/\text{Ne}_{\odot} = 0.90 \pm 0.10$, $\text{Mg}/\text{Mg}_{\odot} = 0.64 \pm 0.10$, $\text{Si}/\text{Si}_{\odot} = 0.66 \pm 0.08$, $\text{S}/\text{S}_{\odot} = 1.01 \pm 0.25$, and $\text{Fe}/\text{Fe}_{\odot} = 0.38 \pm 0.04$, all the other abundances were set to solar values. These results, especially the hydrogen column density, are in general good agreement with the results of Park et al. (2012). We use the hydrogen column density we inferred from this fit as a fixed parameter when analyzing the spectra of SGR 0526–66 in the remainder of the paper.

We simultaneously fit all six spectra with the STEMS model. STEMS model assumes a fully ionized and strongly

¹ http://cxc.harvard.edu/ciao/ahelp/chandra_repro.html

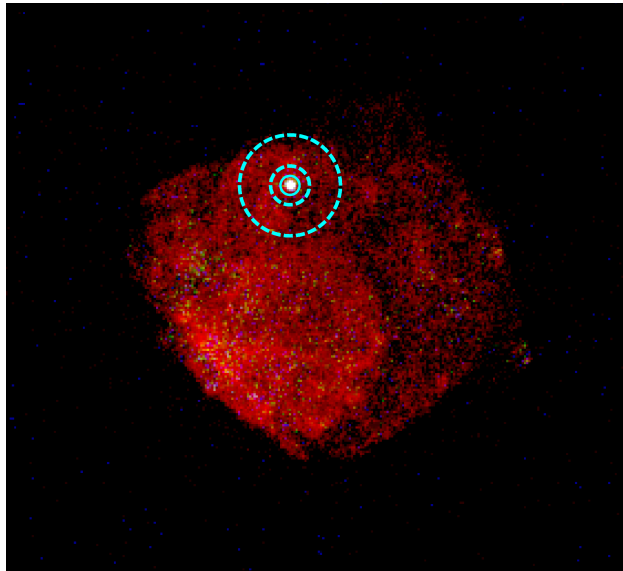


Figure 1. True color image of the supernova remnant N49. Red, green and blue corresponds to the 0.2-2.0, 2.0-4.0 and 4.0-10.0 keV ranges, respectively. Source (solid line) and SNR (dashed lines) extraction regions are also shown in cyan.

magnetized hydrogen atmosphere on the surface of the neutron star, which determines the general spectral characteristics of its X-ray emission (Özel 2001, 2003). In the magnetosphere, these surface photons are further scattered by mildly relativistic charges (Lyutikov & Gavriil 2006). The model has four parameters: the effective temperature, magnetic field strength at the surface as well as the resonant scattering optical depth and the velocity of charged particles in the neutron star magnetosphere (see e.g., Güver et al. 2007, 2008, 2011 for details). First, we allowed all STEMS parameters to vary in all observations. Such a fit resulted in a χ^2/dof of 1.074 for 515 degrees of freedom (dof). Resulting effective surface temperature (~ 0.35 keV), magnetic field strength ($\sim 3.61 \times 10^{14}$ G), the magnetospheric scattering optical depth (~ 5.66) and the average particle velocity (~ 0.55) did not show statistically significant or systematic variations between different observations. However, due to rather low signal to noise ratio of individual X-ray spectra, the error in individual model parameters were large. In order to obtain more constrained results on the effective temperature (therefore, the apparent emitting radius) and follow its time evolution, we linked the model parameters for magnetic field strength, magnetospheric scattering optical depth and the average particle velocity. This way, we obtained a χ^2/dof of 1.086/530. We note here that, despite adding more dof to the fit, the change in the fit statistics was negligible, further indicating that the other parameters do not show statistically significant variations. We obtained the following best fit parameter values when only the surface effective temperature and model normalization were allowed to vary between observations: the surface magnetic field strength $B = (3.74^{+0.11}_{-0.14}) \times 10^{14}$ G, magnetospheric optical depth to resonant scattering $\tau = 5.37^{+0.58}_{-0.44}$, the average velocity of particles $\beta = 0.52 \pm 0.03$. We then used the *cflux* model to calculate the unabsorbed X-ray flux in the 0.5–6.5 keV range for each observation. We present these flux measurements together with the effective surface temperature values for each observation in Table 2. We also show in Figure 2

the 68% confidence contours for the surface effective temperature and flux values. Both Figure 2 and Table 2 show that although the X-ray flux of SGR 0526–66 decreases by a factor of 20% over the last 9 years the inferred temperature values are fairly constant during this period.

Given the fact that the surface temperature remains constant, we repeated our simultaneous fit by linking the surface effective temperature among all observations as well, in order to further constrain it and allowed the normalization, hence the emitting area of the STEMS model, to vary between observations. This way we obtained a χ^2/dof of 1.083/535. Figure 3 shows the data together with the best fitting model and fit residuals. As expected, the best fit values are very similar to what we found earlier: We obtain that the magnetic field strength at the surface is $B = (3.73^{+0.08}_{-0.16}) \times 10^{14}$ G, the optical depth to resonant scattering at the neutron star magnetosphere is $\tau = 5.47^{+0.75}_{-0.49}$ and the average velocity of the magnetospheric particles is $\beta = 0.52 \pm 0.03$ and an effective temperature of $0.355^{+0.031}_{-0.024}$ keV. We note that the best fit value of the surface temperature does not significantly depend on the fixed hydrogen column density. Even when we allow the hydrogen column density to be a free parameter in the fit to the spectra of SGR 0526–66, we obtain a value of $N_H = (0.144 \pm 0.012) \times 10^{22}$ cm⁻², which is consistent with the value we obtained from analyzing the spectrum of the surrounding supernova remnant. The unabsorbed flux and the emitting radius values obtained from this fit is given in Table 2. In Figure 4, we present χ^2/dof contours over the surface effective temperature and magnetic field strength.

4 TIMING ANALYSIS

We performed timing analysis using all available CXO observations to determine the spin period evolution of SGR 0526–66 and to uncover variations in the pulsed fraction. The time resolution of CXO observations in various

Table 2. X-ray spectral fit results for SGR 0526–66.

Date	Unabsorbed Flux ^a (10 ⁻¹² erg s ⁻¹ cm ⁻²)	kT_{eff}^a (keV)	Unabsorbed Flux ^b (10 ⁻¹² erg s ⁻¹ cm ⁻²)	Radius ^b (km)
2000-01-04	1.33±0.02	0.37 ^{+0.04} _{-0.04}	1.31±0.02	13.33±1.56
2001-08-31	1.28±0.02	0.36 ^{+0.04} _{-0.04}	1.26±0.01	13.09±1.54
2009-07-18	1.06±0.02	0.36 ^{+0.05} _{-0.04}	1.04±0.02	11.88±1.37
2009-07-31	1.09±0.03	0.35 ^{+0.05} _{-0.04}	1.07±0.02	12.05±1.39
2009-09-16	1.04±0.02	0.37 ^{+0.03} _{-0.05}	1.00±0.02	11.71±1.35
2009-09-19	1.05±0.02	0.34 ^{+0.04} _{-0.03}	1.03±0.02	11.85±1.37

^a Calculated from each individual data set when all the model parameters were linked between the observations, except for the effective temperature and normalizations.

^b Calculated from each individual data set when all the model parameters were linked between the observations, except for normalizations.

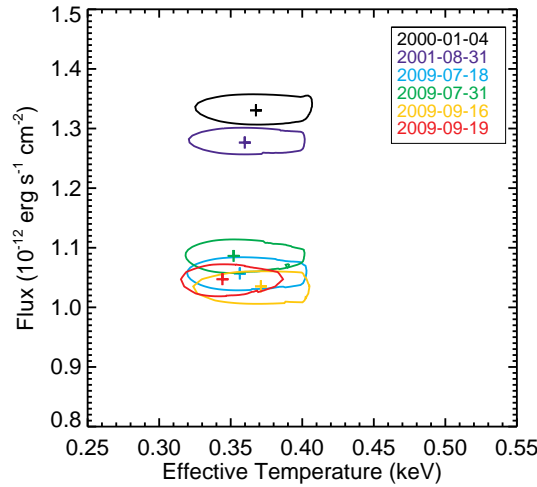


Figure 2. 68% confidence contours of unabsorbed 0.5 - 6.5 keV flux and surface effective temperature values for individual data sets when all other parameters were linked between different observations.

sub-array modes is approximately 0.4 or 0.8 s, which is not ideal but sufficient for timing purposes. Using the same selection regions described in Section 3, we extracted source events for each observation and applied barycentric correction using the *axbary* tool.

We also included the deep XMM-Newton observation performed in 2007 (ObsID 0505310101) in our timing investigation. We calibrated the EPIC-pn data using SAS v.10.0.0 and the calibration files as of October 2010. We extracted source events from a circular region with 10'' radius. Note that the point spread function of XMM-Newton is not accurate enough to completely resolve the pulsar from the supernova remnant; therefore, some fraction of unpulsed emission is expected to originate from the remnant (see Tiengo et al. 2009 for the details of contribution from the supernova remnant). We used the *barycen* tool of SAS to convert each event arrival times to that of the Solar system barycenter.

To search for the pulsed signal from SGR 0526–66, we employed a Z_m^2 technique (Buccheri et al. 1983) with the number of harmonics set to $m = 2$. We performed the search in a period range between 8.0 and 8.1 s. We detect the pulsed signal with high significance in the first three CXO

data sets as well as in the XMM-Newton data, while the detections in the CXO data sets with observation IDs 10806, 10807 and 10808 were marginal. In Table 3, we present only the statistically significant measurements of the spin period of SGR 0526–66, together with the chance probability and the Z_m^2 power of each measurement. To determine the rate of change of the spin period, we fit the measured periods with a first order polynomial. We obtain a good fit with a spin down rate of $(4.019 \pm 0.494) \times 10^{-11} \text{ s s}^{-1}$. We present the evolution of the spin period as well as the best fit spin down rate of SGR 0526–66 in Figure 5. Note that our result regarding the spin evolution is based on only four measurements obtained over nine years. A more precise measurement of the spin down rate require more frequent deep observations.

Finally, we constructed the pulse profile and calculated the root-mean-square pulsed fraction for each observation with significant spin period detection. The rms pulsed fraction (PF) is calculated as,

$$PF = \left(\frac{1}{N} \left(\sum_{i=1}^N (R_i - R_{\text{ave}})^2 - \Delta R_i^2 \right) \right)^{\frac{1}{2}} / R_{\text{ave}}, \quad (1)$$

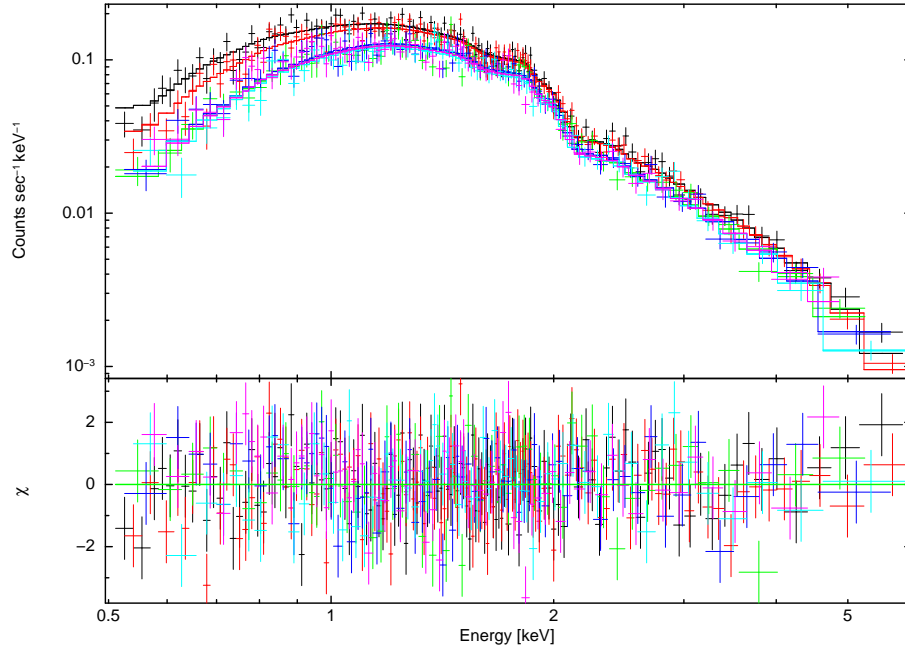


Figure 3. All six X-ray spectra of SGR 0526–66 obtained since 2000 (crosses), best fitting model curves (solid lines) and the fit residuals (lower panel).

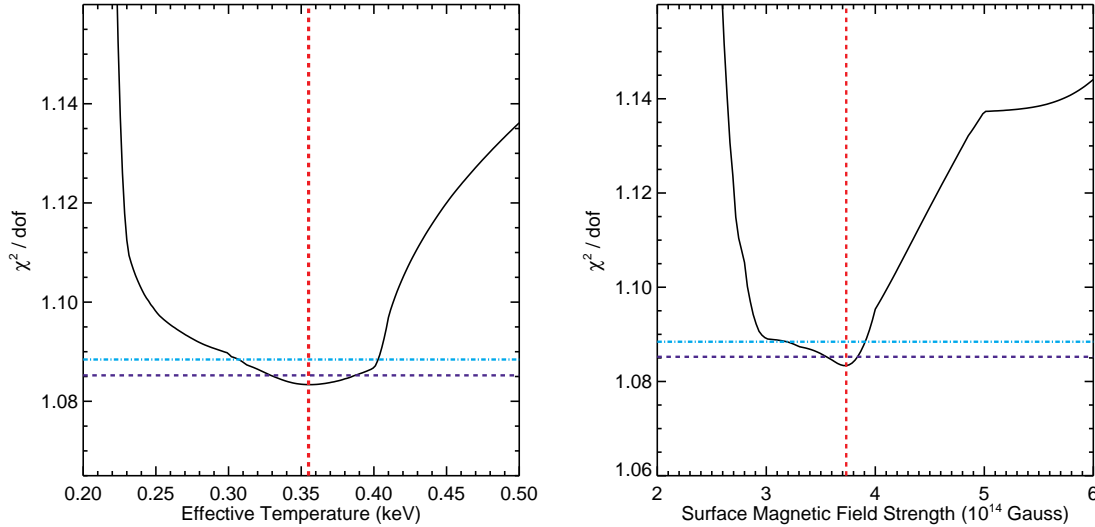


Figure 4. Variations of χ^2/dof as a function of surface effective temperature (left panel) and magnetic field strength (right panel) as inferred from the X-ray spectral fit. Dashed and dashed-dotted lines indicate the 68% and 90% confidence levels for each parameter.

where N is the number of pulse phase bins ($N=16$), R_i is the source count rate in each phase bin, ΔR_i is the associated uncertainty in the count rate, and R_{ave} is the average count rate of the pulse profile. We present the rms pulsed fraction values in Table 3. We find that rms pulsed fraction of SGR 0526–66 is very low and remains constant around 4% among CXO observations, while pulsed fraction obtained from XMM-Newton observation is significantly lower ($\sim 1.5\%$). Note, however, the fact that the rms pulsed fraction value is normalized by the average count rate of the pulse profile and any blended emission from the supernova remnant would increase the average rate and reduce

the pulsed fraction. It is likely that the drop of rms pulsed fraction only seen in XMM-Newton observation is not intrinsic to the source.

5 DISCUSSION AND CONCLUSIONS

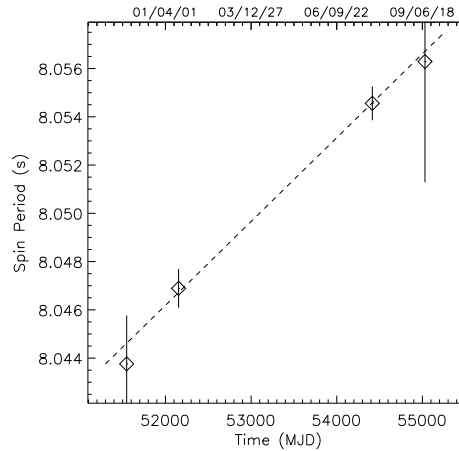
We performed a systematic analysis of the archival Chandra observations of SGR 0526–66. Fitting the X-ray spectra with a strongly magnetized atmosphere model allowed us determine the strength of the surface magnetic field as $B = 3.73 \times 10^{14}$ G and the effective temperature as

Table 3. Results of the timing analysis

Obs ID	Obs Date (MJD)	P_{spin}^a (s)	Maximum Z_2^2 Power	Probability ^b	Pulsed Fraction ^a
747	52415.400	8.044(2)	19.796	5.5×10^{-4}	0.038(10)
1957	52030.200	8.0469(8)	24.518	6.3×10^{-5}	0.042(9)
XMM	55044.000	8.0546(7)	19.027	7.8×10^{-4}	0.015(4)
10123	55090.500	8.056(5)	15.130	4.5×10^{-3}	0.044(14)

^a68% confidence limits of the measurements are in the last digit and given in parentheses.

^bProbability of obtaining the peak power in the Z_2^2 power spectrum if there was no periodic signal present.

**Figure 5.** Spin period history of SGR 0526–66.

0.355 keV. We also obtained the optical depth to resonant scattering in the magnetosphere, $\tau=5.47$, and the average velocity of the magnetospheric particles, $0.52c$. All these parameters remain constant over the course of nine years within uncertainties.

What has been observed to change over this interval is the source flux: it decreased by about 20% from 2000 to 2009 (see also Park et al. 2012). Such a flux decay can result from a ≈ 5 -6% decrease in the surface temperature. This variation is comparable to the uncertainties in individual temperature measurements at the 1 - σ level. Therefore, we can not unambiguously rule out a variation in the temperature. Nevertheless, no systematic variation in the best fit values of the surface temperature has been observed over the nine years. Therefore, it is likely that the surface temperature of SGR 0526–66 remained constant throughout this period.

The decline in the observed flux can also be achieved with a decrease in the radius of the emitting region by about 10%. We obtain through our spectral fits that the radius was about 13.3 km in 2000/2001, and about 11.7 km in 2009, assuming a distance 48.1 kpc (Macri et al. 2006). It is possible that the thermally emitting hot spot on the surface of the neutron star might still carry the effects of burst induced heating in the late 70s and early 80s and dissipates over time without going through a major change in its temperature. It is important to note that the large radius values we deduce from the spectral fits are in agreement with the very low rms pulsed fractions we inferred from the timing analysis.

We determined the spin period history of SGR 0526–66, which is in accord with the results of Tiengo et al. (2009) and derived the period derivative as $4.02 \times 10^{-11} \text{ s s}^{-1}$. Assuming that the spindown of the neutron star is due to a magnetic dipole braking, the inferred dipole magnetic field strength of the neutron star is calculated as $\approx 5.7 \times 10^{14} \text{ G}$, which agrees with the surface magnetic field strength as found from the X-ray spectra using the STEMS model. Making the same spindown assumption, we calculate the characteristic age of the pulsar as $\tau_{sd} = P/2\dot{P} \approx 3200 \text{ yr}$. This is comparable to, but somewhat lower than, the estimated Sedov age of the supernova remnant, which is 4800 yr (Park et al. 2012). Because SGRs and AXPs exhibit episodic variable spindown behavior (see, e.g., Woods et al. 2002), the characteristic age should only be taken as a rough indicator of the true age of SGR 0526–66. If SGR 0526–66 is indeed associated with N49, it requires a rather high radial velocity for the neutron star compared to some other AXPs and SGRs (Gaensler et al. 2001; Kaplan et al. 2009).

Long term observations of magnetars may play an important role in our understanding of the magnetic field decay and its effects on the neutron star crust and long term cooling. However, observations of magnetars over the last couple of decades showed that these neutron stars are rarely in quiescent state: They show giant flares (Hurley et al. 1999; 2005), outbursts (Ng et al. 2011), glitches (Dib et al. 2007), which likely affect the long-term cooling prevent any observational constrains on the theoretical calculations. Although located at a large distance and residing within a

SNR, SGR 0526–66 is an exception in this regard. Since the giant flare observed in 1979 and the bursting activity that lasted till 1983, no burst activity has been reported from this source, enabling us to assume that the source has been steadily cooling in quiescence. This is also confirmed by our spectral results presented in Section 3. One other advantage of this source is its possible association with the supernova remnant N49, providing a reasonable age estimate for the neutron star.

Aguilera et al. (2008a) calculated cooling curves for strongly magnetized neutron stars by taking into account the Ohmic dissipation (τ_{Ohm}) and Hall drift (τ_{Hall}) processes, where the latter is employed for a rapid decay during early stages (see eq. 17 in Aguilera et al. 2008a). We can compare our results with the magnetic neutron star cooling curves calculated by Aguilera et al. (2008a, b) by using a conservative age range for SGR 0526-66, together with the surface temperature that we determined from six Chandra observations covering nearly a 10 year time interval. We take the age of the neutron star to be 3000–7000 yr, which spans the spindown age of SGR 0526-66 and the supernova remnant age reported by Park et al. (2003, 2012). In Figure 6, we present the cooling curves for magnetars with various initial magnetic field strengths, along with the current surface temperature of SGR 0526–66. Our comparison shows the cooling trend of SGR 0526–66 matches the theoretical cooling curves corresponding to two sets of parameters, an initial magnetic field strength of 10^{16} G, τ_{Ohm} of 10^6 yr and $\tau_{\text{Ohm}}/\tau_{\text{Hall}} = 5 \times 10^2$ yr, or the curve that corresponds to an initial magnetic field strength of 1.5×10^{15} G, τ_{Ohm} of 10^6 yr and $\tau_{\text{Ohm}}/\tau_{\text{Hall}} = 5 \times 10^3$ yr.

On either cooling track, SGR 0526–66 is expected to enter a phase of more rapid cooling in the near future, based on its age and its current temperature, which we reported here. If its temperature indeed begins to decay rapidly, observations of the source over the next decade with planned X-ray telescopes, such as Advanced Telescope for High Energy Astrophysics, may reveal a more significant drop in the spectral temperature, accompanied by a further flux decay, as long as the source remains in its deep quiescence.

ACKNOWLEDGMENTS

We thank Deborah Aguilera and Jose Pons for sharing their theoretical calculations on the cooling of magnetars. We thank the referee for insightful suggestions that improved the clarity of the manuscript. TG acknowledges support from the Scientific and Technological Research Council of Turkey (TÜBİTAK BİDEB) through a fellowship programme.

REFERENCES

- Aguilera, D. N., Pons, J. A., & Miralles, J. A. 2008, *A&A*, 486, 255
 Aguilera, D. N., Pons, J. A., & Miralles, J. A. 2008, *ApJL*, 673, L167
 Aptekar R. L., Butterworth P. S., Cline T. L., Frederiks D. D., Golenetskii S. V., Il'Inskii V. N., Mazets E. P., Pal'Shin V. D., 2002, *MmSAI*, 73, 485

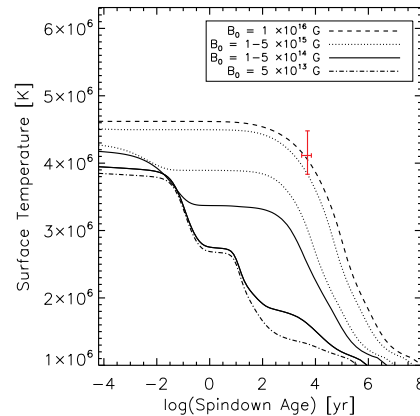


Figure 6. Surface temperature of SGR 0526–66 inferred using the STEMS model together with a plausible age range (red cross sign) overplotted to surface temperature at the pole as a function of spindown age for magnetars with different initial magnetic field strengths as calculated by Aguilera et al. (2008a, b).

- Arnaud, K. A. 1996, in *Astronomical Society of the Pacific Conference Series*, Vol. 101, *Astronomical Data Analysis Software and Systems V*, ed. G. H. Jacoby & J. Barnes, 17
 Bilikova J., Williams R. N. M., Chu Y.-H., Gruendl R. A., Lundgren B. F., 2007, *AJ*, 134, 2308
 Borkowski K. J., Lyerly W. J., Reynolds S. P., 2001, *ApJ*, 548, 820
 Buccheri R., et al., 1983, *A&A*, 128, 245
 Duncan R. C., Thompson C., 1992, *ApJ*, 392, L9
 Durant M., van Kerkwijk M. H., 2006, *ApJ*, 650, 1082
 Evans, W. D., et al. 1980, *ApJL*, 237, L7
 Gaensler B. M., Slane P. O., Gotthelf E. V., Vasisht G., 2001, *ApJ*, 559, 963
 Güver, T., Özel, F., Göğüş, E., & Kouveliotou, C. 2007, *ApJL*, 667, L73
 Güver, T., Özel, F., Göğüş, E. 2008, *ApJ*, 675, 1499
 Güver T., Göğüş E., Ö-Zel F., 2011, *MNRAS*, 418, 2773
 Guver T., Psaltis D., Ozel F., 2011, *ApJ* in press, arXiv:1103.5767
 Özel, F., Güver, T., Göğüş, E. 2008, *40 Years of Pulsars: Millisecond Pulsars, Magnetars and More*, 983, 254
 Kaplan D. L., Chatterjee S., Hales C. A., Gaensler B. M., Slane P. O., 2009, *AJ*, 137, 354
 Kulkarni, S. R., Kaplan, D. L., Marshall, H. L., Frail, D. A., Murakami, T., & Yonetoku, D. 2003, *ApJ*, 585, 948
 Lyutikov, M., & Gavriil, F. P. 2006, *MNRAS*, 368, 690
 Macri L. M., Stanek K. Z., Bersier D., Greenhill L. J., Reid M. J., 2006, *ApJ*, 652, 1133
 Mazets, E. P., Golenskii, S. V., Ilinskii, V. N., Aptekar, R. L., & Guryan, I. A. 1979, *Nature*, 282, 587
 Mereghetti S., 2008, *A&ARv*, 15, 225
 Ng C.-Y., et al., 2011, *ApJ*, 729, 131
 Özel, F. 2003, *ApJ*, 583, 402
 Özel, F. 2001, *ApJ*, 563, 276
 Park S., Burrows D. N., Garmire G. P., Nousek J. A., Hughes J. P., Williams R. M., 2003, *ApJ*, 586, 210
 Park S., Hughes J. P., Slane P. O., Burrows D. N., Lee J.-J., Mori K., 2012, arXiv, arXiv:1201.5056, accepted by

- ApJ
Rea N., Zane S., Turolla R., Lyutikov M., Götz D., 2008,
ApJ, 686, 1245
Rea N., Esposito P., 2011, *heep.conf*, 247
Rothschild R. E., Kulkarni S. R., Lingenfelter R. E., 1994,
Natur, 368, 432
Tiengo, A., et al. 2009, MNRAS, 399, L74
Woods P. M., Kouveliotou C., Göğüş E., Finger M. H.,
Swank J., Markwardt C. B., Hurley K., van der Klis M.,
2002, ApJ, 576, 381
Woods P. M., Thompson C., 2006, *csxs.book*, 547